EPJ Photovoltaics **13**, 8 (2022)

https://doi.org/10.1051/epjpv/2022005

Available online at:
www.epj-pv.org

REGULAR ARTICLE OPEN ACCESS

Hydrogenation of sputtered ZnO:Al layers for double side poly-Si/SiO_x solar cells

Charles Seron[1,2,*], Thibaut Desrues[1], Frédéric Jay[1], Adeline Lanterne[1], Frank Torregrosa[3], Gaël Borvon[3], Quentin Rafhay[2], Anne Kaminski[2], and Sébastien Dubois[1]

[1] Univ. Grenoble Alpes, CEA, LITEN, DTS, SCPV, F-73370 Le Bourget-du-Lac, France
[2] Univ. Grenoble Alpes, Univ. Savoie Mont-Blanc, CNRS, Grenoble INP, IMEP-LAHC, 38000 Grenoble, France
[3] Ion Beam Services, Rue Gaston Imbert Prolongé, ZI Rousset-Peynier, 13790 Peynier, France

Received: 30 June 2021 / Received in final form: 11 February 2022 / Accepted: 21 February 2022

Abstract. This work presents the development and the application of innovative and sustainable transparent conductive oxide (TCO) materials for contacting polysilicon (poly-Si) on oxide (SiO_x) stacks used as passivating contacts in solar cell devices. Adding hydrogen into ZnO:Al (AZO) layers deposited by magnetron sputtering potentially leads to a twofold positive effect. First, it brings hydrogen atoms into the layers, which can enhance both electrical and optical material properties of the TCO. Second, hydrogen can significantly improve cell performances, by fixing dangling bonds at the SiO_x/substrate interface and by passivating bulk defects. *In situ* and *ex situ* hydrogenation processes have been compared on those multiple aspects with investigation about anneals at 350 °C. AZO layers have been successfully integrated on the front side of complete solar cells featuring poly-Si/SiO_x-based passivating contacts, leading to a record conversion efficiency of 22.4% for a cell with AZO. The results show that using AZO instead of an indium based TCO is suitable for passivated contacts solar cell with high temperature route. Thus, it increases the credibility towards large-scale deployments of TCO-based high efficiency silicon solar cells in terms of cost and resources.

Keywords: Transparent conductive oxide / indium-free/aluminum zinc oxide / passivated contacts / poly-Si / SiO_x

1 Introduction

The double side integration of polysilicon on oxide based passivated contacts is a promising way to improve the performances of crystalline silicon (c-Si) solar cells [1–3]. With such a double-side passivated contacts configuration, the collecting layers (i.e., poly-Si films) must be as thin as possible to limit parasitic absorption of incident light [4,5]. A full surface contact by a transparent conductive oxide layer (TCO) is thus usually required, as presented on the solar cell architecture of Figure 1, where active layers have a thickness inferior to 20 nm. If indium-based TCO layers are known for their excellent electrical and optical properties, issues about indium cost and scarcity are pushing the PV community to investigate new solutions [6,7]. Compared to standard silicon heterojunction solar cells using hydrogenated amorphous silicon (a-Si:H) layers, the high temperature route with polysilicon on oxide structure benefits from several assets for using alternative TCO materials. For instance, poly-Si layers feature higher lateral conductivity values (in comparison with a-Si:H), which could reduce the constraints on the TCO properties. It is especially the case in rear emitter configuration, as it is the case in Figure 1 [8]. However, the formation of poly-Si based structures implies a high temperature (>800 °C) annealing for crystallization and dopants activation. This annealing step causes the partial effusion of hydrogen, which can passivate interfaces, crystal defects and impurities [9] out of the silicon wafer. It is particularly problematic in the case where hydrogen atoms were previously incorporated at the surface/bulk during deposition or doping treatments. In this study, Plasma Immersion Ion Implantation (PIII) with PH_3 and B_2H_6 precursors is respectively used for phosphorus and boron doping of polysilicon layers. After dopants activation annealing, the effective carrier lifetime is limited due to recombination at unpassivated defects (surface and bulk) [10]. To reach higher passivation levels, hydrogenation processes could be used after this high temperature annealing.

In this work, addition of hydrogen into aluminum-doped zinc oxide ZnO:Al (AZO) layers is studied as an

* e-mail: charles.seron@cea.fr

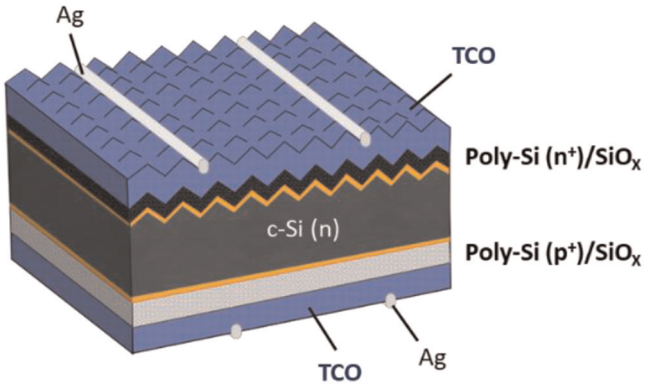

Fig. 1. c-Si solar cell structure in rear emitter configuration with double side passivated contacts elaborated by high (poly-Si/SiO_x) temperature route.

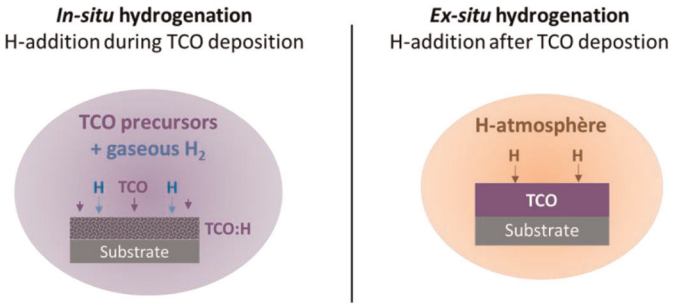

Fig. 2. Schematic view of deposition-free *in situ* and *ex situ* hydrogenation of TCO layers.

alternative to indium based TCO and to improve solar cell performances. Indeed, hydrogenation treatments on TCO can improve their electrical and optical properties [11]. Moreover, thanks to their high diffusivity, hydrogen atoms initially present inside TCO layers could diffuse towards the underlaying materials and interfaces, especially with thermal treatments, thus lowering the carrier recombination rates.

Two ways of hydrogen addition into TCO layer have been in particularly explored: *ex situ* addition, with the use of Hydrogen-Plasma Immersion Ion Implantation (PIII-H_2), and *in situ* hydrogenation, where hydrogen is added into the layer during its deposition. Schematic representation of both hydrogenation processes are depicted in Figure 2.

In situ incorporation of hydrogen prevents the need for additional hydrogenation process steps, whereas *ex situ* method imply an additional step. However, use of PIII-H_2 allows a fine tuning of concentration and profile of implanted hydrogen atoms. Plasma Immersion Ion Implantation has been shown to be particularly promising as doping technique for photovoltaic devices [12,13].

It is worth noting that another way for *ex situ* hydrogenation consists in the deposition of a hydrogen rich dielectric layer onto the TCO layer [14,15]. However this hydrogenation method brings difficulties in contacting TCO layers with front grid electrode.

In this study, effects of both deposition-free in and *ex situ* hydrogenation processes will be therefore investigated with electrical, optical and effective lifetime measurements. Besides, double-side passivated contacts solar cells will be fabricated. This will allow to assess the impact of TCO way of hydrogenation on the performances of complete photovoltaic devices.

2 Experimental results

2.1 TCO deposition and hydrogenation processes

ZnO:Al layers were deposited by magnetron sputtering with a Jusung equipment. For *in situ* hydrogenation, deposition chamber atmosphere consists in a mix between pure Ar or Ar:H_2 (98:2%) and O_2 gases. The total gas flowing in the chamber is fixed at 600 sccm and the O_2 flow is also set at 1% of the chamber composition. Repartition between Ar and Ar:H_2 converging to the deposition chamber can be modified to reach total compositions in hydrogen in the chamber of 0% (corresponding to standard AZO layer without hydrogen addition), 0.5%, 1% and 1.5%. The different AZO:H layers will be distinguished by the H_2 amount used during deposition.

For *ex situ* hydrogen addition, standard AZO layer is deposited, i.e. with only pure Ar and O_2 flow during deposition. Samples are then placed into a Pulsion Solar® tool to perform hydrogen ion implantation by PIII-H_2. Acceleration voltage from to 0.5 kV to 2 kV and a fixed dose of 1×10^{15} cm^{-2} have been used. Modification of acceleration voltage allows to modify the penetration depth of hydrogen atoms into the top layers. In this present case, it would be an interesting point if hydrogen could be implanted beyond the TCO layers to passivate poly-Si/SiO_x stack. However, ion implantation could generate crystal defects in this implanted region, causing a degradation of substrates used.

For material comparisons, a reference hydrogenated ITO layer is also deposited by magnetron sputtering with an in-line Meyer-Burger Physical Vapor Deposition (PVD) tool. ITO layer is *in situ* hydrogenated, by adding hydrogen to deposition chamber during the process.

2.2 Electrical and optical results after AZO hydrogenation

Corning glass samples of 2×2 cm^2 are used as substrates for electrical and optical characterizations of TCO materials. For these measurements, a TCO layer thickness of 100 nm is targeted. The sheet resistance (R_{sheet}) is then measured by 4-point probes method on a Napson equipment. The charge carriers mobility and concentration values are determined by Hall effect analyses using a Van der Pauw configuration with an Ecopia tool. The transparency of TCO is finally assessed with a Perkin-Elmer spectrophotometer on a large range of wavelengths (from 280 nm to 2400 nm). The TCO-covered samples experienced low temperature annealing step at 350 °C during 5 min under N_2 flow in a Carbolite Gero oven. The previously presented characterizations are conducted after TCO deposition and after annealing.

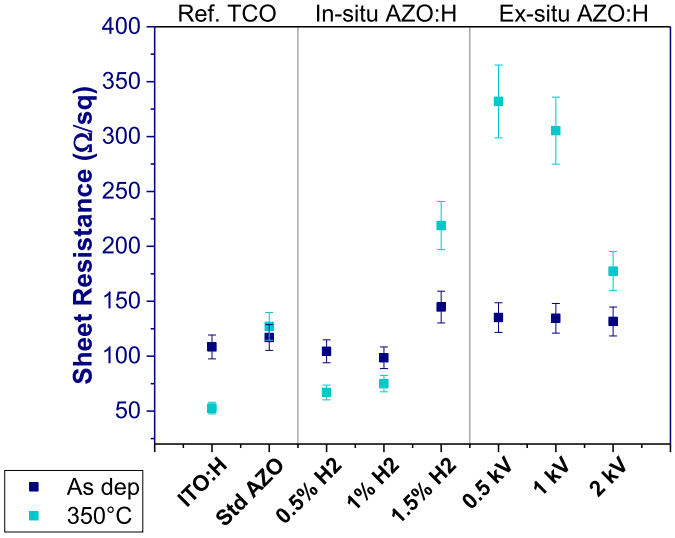

Fig. 3. Variation of R_{sheet} values with the TCO composition and the annealing at 350 °C.

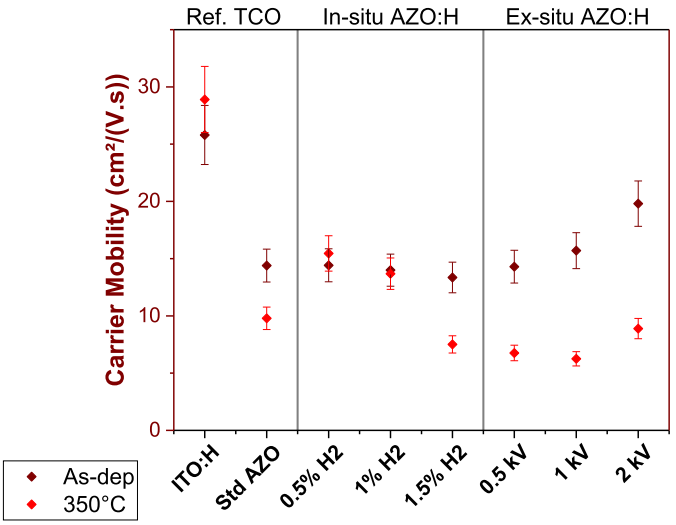

Fig. 4. Variation of charge carrier mobility with the TCO composition and the annealing at 350 °C.

The values of R_{sheet}, charge carrier mobilities and concentrations for different TCO conditions of hydrogenation and annealing are respectively presented in Figures 3–5.

As shown by Figure 3, similar R_{sheet} are obtained after deposition for reference AZO and ITO:H. As deposited, a slight decrease of AZO layer R_{sheet} is measured when hydrogen is *in situ* added into the TCO layer, for both "0.5% H_2" and "1% H_2" AZO. Indeed with 1% H_2, post-TCO R_{sheet} is just below 100 Ω/sq, whereas the value is around 120 Ω/sq for a standard AZO deposited without hydrogen flow. Higher concentration "1.5% H_2" leads to increased values of AZO R_{sheet}, which are similar to R_{sheet} values after AZO hydrogenation by PIII-H_2. For all acceleration voltages studied, TCO layers sheet resistance are indeed close to 150 Ω/sq, which is slightly higher than standard AZO.

Annealing at 350 °C allows to decrease R_{sheet} of hydrogenated ITO and of *in situ* hydrogenated AZO with 0.5% and 1% H_2. As shown by Figures 4 and 5, the R_{sheet} reduction in the case of ITO is mainly due to a charge carrier concentration increase, the concentration exceeding 4.0×10^{20} cm^{-3} after the 350 °C annealing. For *in situ* AZO:H, the main factor of R_{Sheet} reduction is an increase of the charge carrier concentration, approaching 6×10^{20} cm^{-3} ("1% H_2", 350 °C annealing). Notice that this increase in the charge carrier concentration could enhance free carrier absorption (FCA). Therefore, controlling the TCO effective transmission will be paramount for future device integrations. 350 °C annealing steps on other hydrogenation conditions (*in situ* "1.5% H_2" and all *ex situ* conditions result in a decrease of carrier mobility, reaching values below 10 cm^2/(V s). For these layers, there is also a stability of carrier concentration values with annealing step at 350 °C, leading finally to a sheet resistance increase. At 350 °C, this R_{sheet} rise seems however to be limited with the highest acceleration voltage value of 2 kV for *ex situ* hydrogenation.

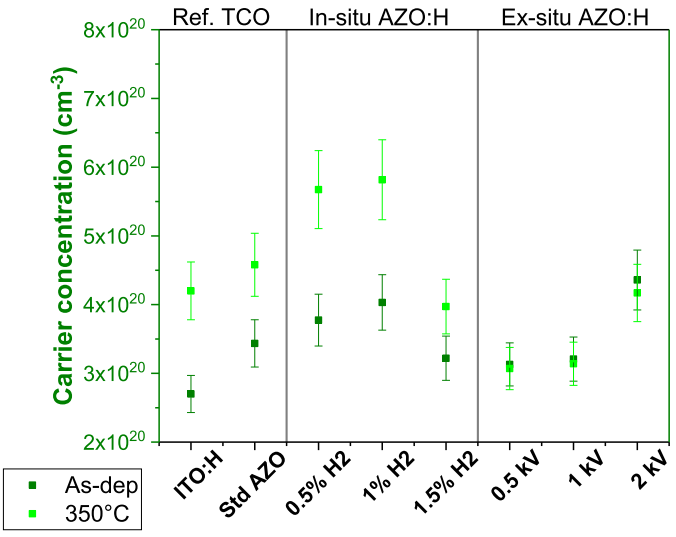

Fig. 5. Variation of charge carrier concentration with TCO composition and annealing at 350 °C.

The effective transmission (T_{eff}) of different AZO layers is presented in Figure 6. This effective transmission is calculated by integrating the transmission spectrum of TCO layer deposited on glass with the AM1.5G solar spectrum on the spectral range from 300 nm to 1200 nm. Hydrogenated ITO layer presents lower effective transmission than all AZO layers. Higher absorption in ITO compared to AZO layers for a similar thickness is due to intrinsic differences between these two materials [16]. It is the case after deposition, where ITO:H T_{eff} is around 79.1% but also after annealing at 350 °C, where it reaches 83.2%. On the contrary, all AZO layers present effective transmission above 80% after deposition. This value increases after annealing for all conditions of deposition, particularly for *in situ* way of hydrogenation. It indeed

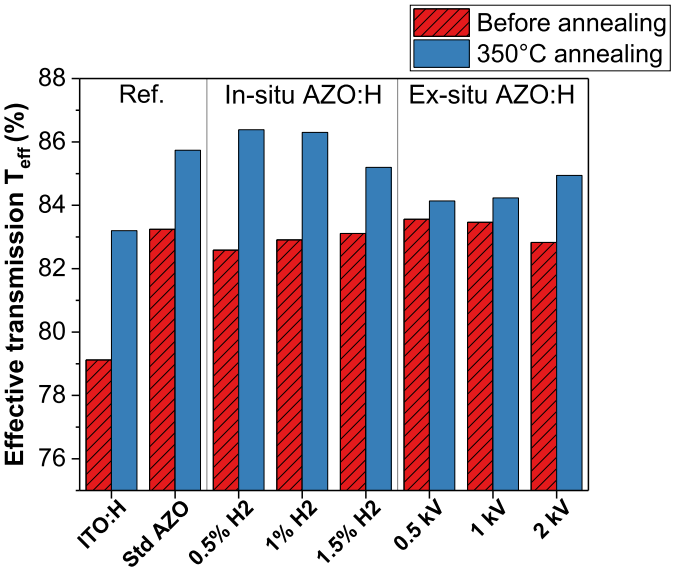

Fig. 6. Evolution of effective transmission depending of TCO hydrogenation, after deposition/hydrogenation and after annealing at 350 °C.

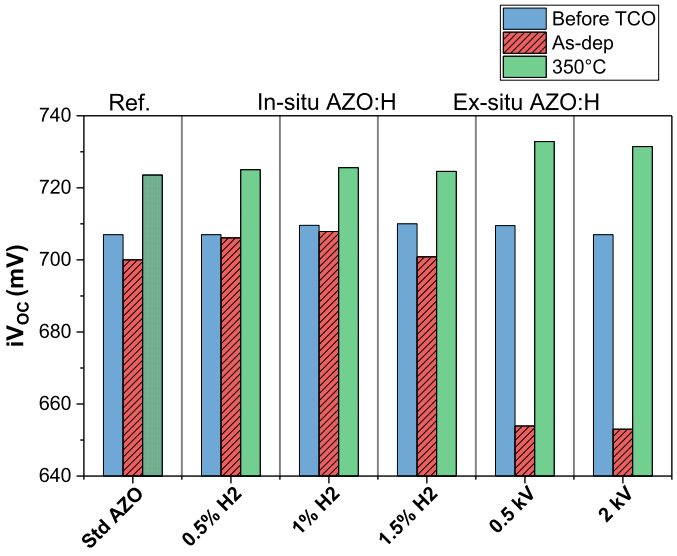

Fig. 7. Variation of iV_{OC} of symmetrical samples featuring poly-Si n^+/SiO_x with TCO layers composition and at different process steps.

reaches more than 86% for 0.5% and 1% H_2 concentration, superior to reference AZO layer without hydrogen at 85.7% of effective transmission. For *ex situ* hydrogenation, maximum T_{eff} values are slightly superior 84% for acceleration voltage of 0.5 kV and 1 kV, and at 85% for 2 kV.

2.3 Passivation behaviour of different TCO layers on symmetrical polysilicon/SiO_x stacks

2.3.1 n^+ symmetrical poly-Si samples

For n^+ poly-silicon layers, n-type ($\rho = 2.1\ \Omega$ cm) M2-Cz-silicon wafers, with a double side KOH-texturization, are used. Then, a 1.5 nm thick thermal oxide is grown followed by the LPCVD double-side deposition of a 15 nm-thick intrinsic polysilicon film on a Hortus platform from Semco Smartech company. Symmetrical doping is then conducted by Plasma Immersion Ion Implantation (PIII) on a Pulsion Solar® equipment from Ion Beam Services (IBS) company. Phosphorus doping is carried out for n^+ poly-Si layers, using an acceleration voltage of 4 kV and PH_3 dose of 7.5×10^{15} at/cm^2. Dopant activation and crystallisation are then performed by an annealing step at 875 °C during 30 min under N_2 flow in a conventional Centrotherm tube furnace. TCO layers are finally deposited on both surfaces. For *ex situ* hydrogenation, a standard AZO layer is implanted using a constant PIII-H_2 dose of 1×10^{15} at/cm^2 and acceleration voltages of 0.5 kV and 2 kV. These *ex situ* conditions have been only studied for n^+ poly-Si layers. The surface passivation level is assessed by extracting the implied open circuit voltage (iV_{OC}) from Photo-Conductance Decay measurements with a Sinton equipment in transient mode (the samples have been found to feature high carrier lifetime, above 200 µs). TCO annealing step at 350 °C under N_2 flow are conducted after first post-deposition measurement on the same samples. The evolutions of iV_{OC} along the successive hydrogenation and annealing for the different samples are presented in Figure 7 for n^+ poly-Si samples.

For standard AZO, an iV_{OC} decrease of 15 mV after TCO deposition is highlighted. This decrease is likely to be due to sputtering damages during the deposition process [17]. With the low *in situ* H_2 concentrations (i.e. 0.5% and 1%), a lower drop due to sputtering damage is observed. However, standard AZO deposition for *ex situ* study causes a dramatical decrease of iV_{OC}. It is important to notice that these depositions were made in another campaign and at a different time than standard AZO and *in situ* AZO:H study. PIII-H_2 process for TCO hydrogenation leads to an increase of this degradation for an acceleration voltage of 0.5 kV, whereas iV_{OC} remains constant when hydrogenated at 2 kV. For all ways of hydrogenation of AZO layers, a complete recovery is yet obtained with annealing at 350 °C. iV_{OC} values even slightly increase at 350 °C, reaching over 720 mV for *in situ* AZO. iV_{OC} values are maximal with *ex situ* way of hydrogenation, with iV_{OC} around 725 mV. In all case, comparing to reference AZO without hydrogen addition, hydrogenation processes appear to have in fact a limited effect on passivation quality on n^+ poly-Si layers.

2.3.2 p^+ symmetrical poly-Si samples

For symmetrical p^+ poly-Si samples, the same wafers are used for effective lifetime measurements than for n^+ poly-Si samples, but with a KOH-polished surface. Further steps are identical, except for intrinsic poly-Si boron doping, where PIII-B_2H_6 is performed with an acceleration voltage of 6 kV and an implantation dose of 7.0×10^{15} at/cm^2. For p^+ poly-Si samples, *ex situ* way of hydrogenation has not been studied, focusing on *in situ* hydrogenation and comparing results with hydrogenated ITO layers behaviour.

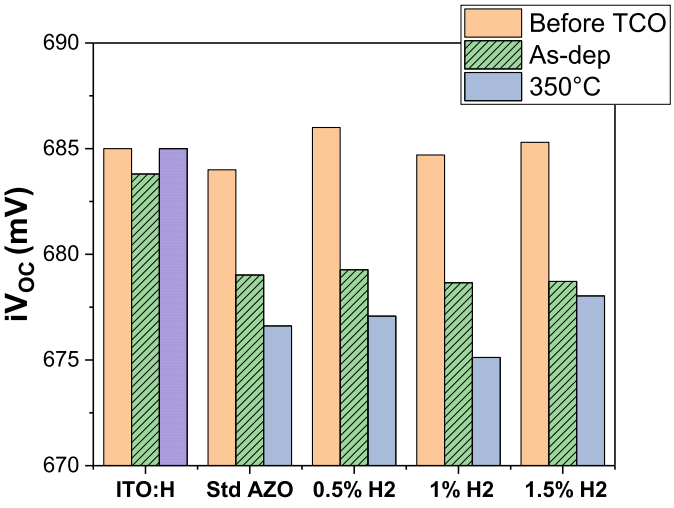

Fig. 8. Variation of iV_{OC} values for symmetrical samples featuring poly-Si p^+/SiO_x with TCO layers composition and at different process steps.

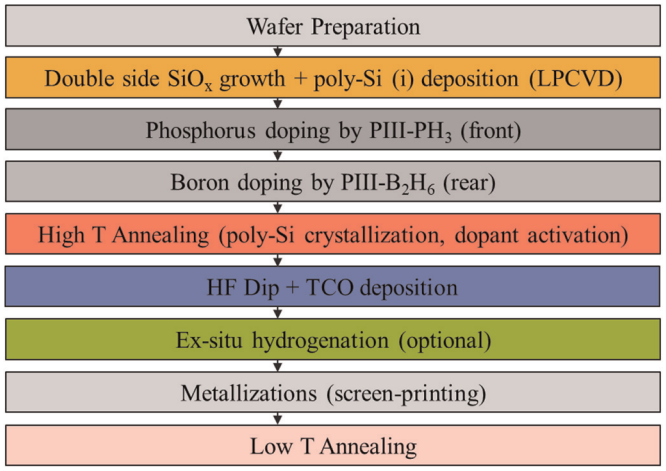

Fig. 9. Fabrication process of double-side poly-Si/SiO_x based passivated contacts solar cell.

The evolution of iV_{OC} as function of TCO composition are presented in Figure 8 for p^+ poly-Si samples. Symmetrical samples without TCO presents iV_{OC} values around 685 mV, which is lower than for n^+ poly-Si samples. p^+ poly-Si layers are nevertheless less sensitive to sputtering damage than n^+ layers. Degradation due to TCO deposition is indeed inferior to 10 mV for all conditions studied. For hydrogenated ITO, sputtering damage only causes an iV_{OC} loss of 3 mV. This first observation can have several explanations. It may be due to a better resistance of p^+ poly-Si layers compared to n^+ counterparts. This can also be due to the deposition surface, which is polished in the case of p^+ poly-Si layers, and could result in a different layer thickness after LPCV-Deposition. Contrary to n^+ poly-Si layers, annealing at 350 °C after TCO deposition causes a slight degradation of iV_{OC} for standard and hydrogenated AZO layers. This annealing loss is bounded to 5 mV, but when adding sputtering and annealing damage, it leads to a total loss of 10 mV for *in situ* AZO:H with 1% H_2 for instance. It is important to notice, that this annealing degradation is not observed with ITO:H layers, which recover with 350 °C annealing, without further gain compared to before the TCO deposition. As discussed for n^+ poly-Si layers, no effect of the hydrogenation processes studied here is observed on passivation quality for p^+ poly-Si layers as well.

2.4 Solar cell integration

Complete solar cell integration has been carried out to confirm the impact of TCO material and hydrogenation process in entire solar cells devices. Figure 9 summarizes the process of fabrication of these cells.

Cell precursors with double-side polysilicon on oxide passivated contacts are prepared to assess the compatibility of the developed indium free TCO with this structure. Wafers similar to those used for the "passivation study" are prepared, with a rear side KOH-polished and a front side KOH-texturized. The same LPCV-Deposition is conducted, followed by front side phosphorus doping, still using PIII-PH_3 with an acceleration voltage of 4 kV and a dose of 7.5×10^{15} at/cm^2. Boron doping is performed at the rear side using an acceleration voltage of 6 kV and a dose of 7×10^{15} at/cm^2. The dopant-activation annealing step at 875 °C during 30 min is the same than the one used in the previous sections.

The hydrogenated AZO layers are integrated only on the front side of the cell and several front TCO are compared: standard AZO, *in situ* hydrogenated AZO with 1% H_2 and *ex situ* hydrogenated AZO by PIII-H_2 using acceleration voltage of 2 kV and a dose of 1×10^{15} at/cm^2. For all these samples, an *in situ* hydrogenated ITO is used for the rear side contact. Moreover, a split featuring a double side integration of standard AZO is fabricated to determine the impact of TCO composition on both sides of the solar cell. For both rear and front side, a TCO thickness of 100 nm is targeted. After TCO deposition, a busbarless electrode-pattern is screen-printed, using a non-firing through silver paste. It must be noted that solar cells with *ex situ* hydrogenation have been printed separately and that a more recent paste evolution has been used, which could lead to minor changes in the contact resistivity and line aspect. The final co-annealing step of TCO and metal electrode is then conducted at 350 °C under N_2 flow during 5 minutes before IV measurements on a Pasan tool.

Complete results of this solar cell integration is presented in Figure 10. Summary of average cells performances with best cell parameters value (in brackets) are presented in Table 1.

2.4.1 Open-circuit voltage (V_{OC}) analysis

Similar V_{OC} are obtained with the different TCO layers, due to the recovery of the post-TCO-deposition damages when annealing at 350 °C for front side integration of AZO layers, as it has been observed in passivation study on n^+ type substrate. It leads to values superior to 700 mV for almost all fabricated cells. Rear side AZO hence do not lead to a degradation of V_{OC} value, contrary to what has been observed regarding the passivation on p^+ type poly-Si. Front side *in situ* hydrogenated AZO moreover present

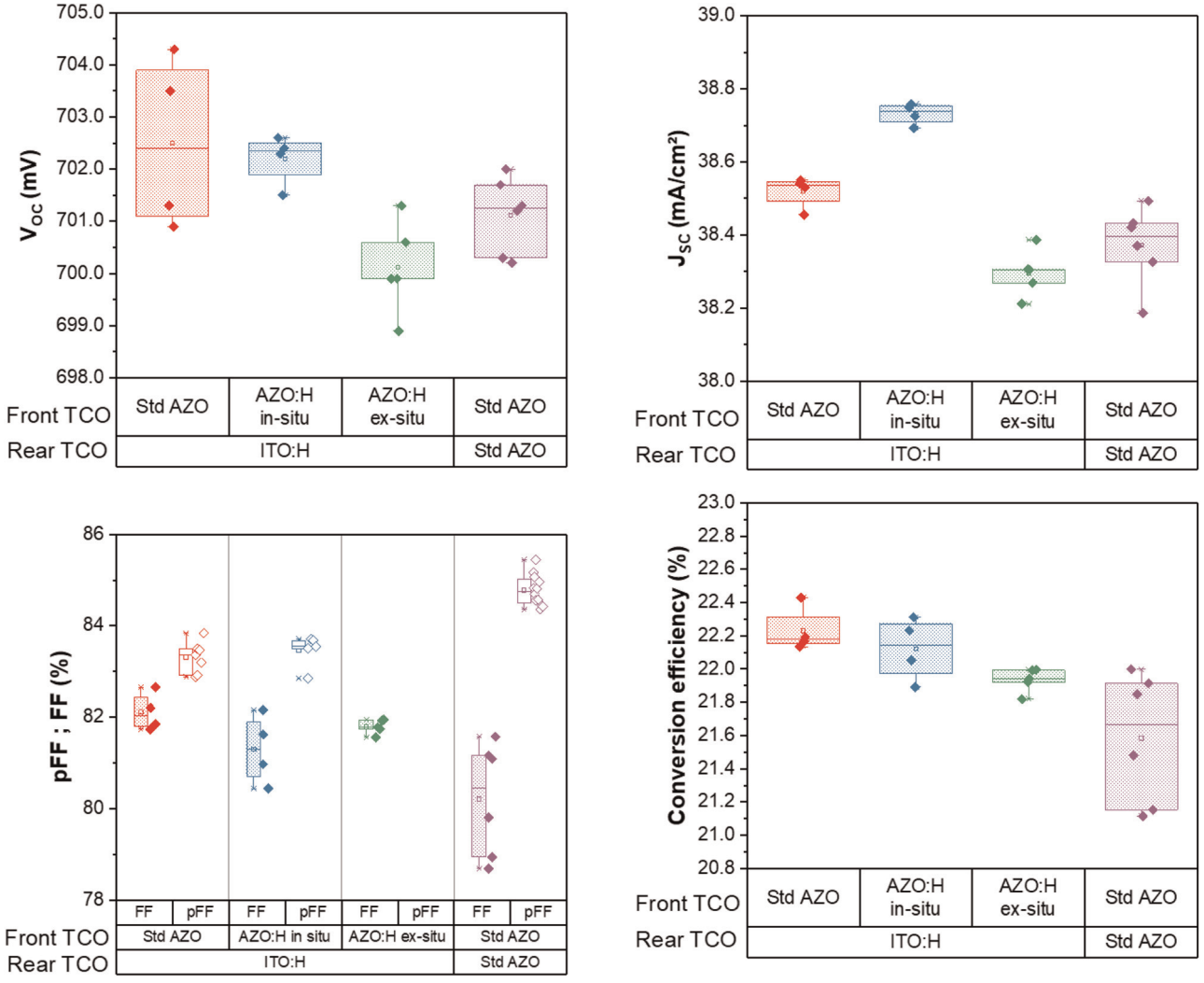

Fig. 10. Cell parameters obtained (V_{OC}, J_{SC}, FF and conversion efficiency) for different structure of solar cells fabricated.

Table 1. Summary of cell performances obtained for solar cell fabricated.

Rear TCO	Front TCO	V_{OC} (mV)	J_{SC} (mA/cm^2)	FF (%)	Efficiency (%)
ITO:H	Std AZO	702.5 (703.5)	38.52 (38.55)	82.11 (82.66)	22.23 (22.43)
ITO:H	AZO:H *ex situ*	700.1 (700.6)	38.30 (38.93)	81.79 (81.77)	21.93 (22.00)
ITO:H	AZO:H *in situ*	702.2 (701.5)	38.73 (38.69)	81.30 (82.15)	22.12 (22.31)
Std AZO	Std AZO	701.1 (702.0)	38.37 (38.49)	80.21 (81.58)	21.58 (22.00)

reduced dispersion of iV_{OC} values all contained between 701.5 and 703.0 mV.

2.4.2 Short-circuit current density (J_{SC}) analysis

J_{SC} values obtained are fitting well with effective transmission calculated from spectrophotometry experiments. Cells with hydrogenated AZO by PIII-H_2, which presented the lowest effective transmission after annealing at 350 °C, exhibit also the lowest J_{SC} values slightly higher than 38.2 mA/cm^2, while the better J_{SC} values are obtained with front *in situ* hydrogenated AZO, reaching 38.8 mA/cm^2. Cells with standard AZO layer without hydrogen addition at the front, lead to intermediate J_{SC} values of 38.5 mA/cm^2.

2.4.3 Fill factor (FF) analysis

Variation of fill factor for different samples features interesting trends. Average values are much higher when using AZO layers at the front side only. With double side standard AZO, average value for fill factor is 80.4%, whereas this average value is above 81% when using hydrogenated ITO at the rear side. This difference is likely to be due to the excellent properties of ITO:H layers, which exhibit very low sheet resistivity and high charge carrier mobility, well suited for contacting a rear side emitter solar cell. This lower average is also due to a large dispersion of FF values for double side AZO.

Focusing on only front AZO integration, high fill factor values are obtained with standard AZO at the front side (82.1% average). *Ex situ* hydrogenated AZO, with very low values dispersion present average FF at 81.9%. Lower average values are obtained for *in situ* hydrogenated AZO layers on the cell front side (81.4%). Notice that at cell level, FF values of AZO layers integrated on front side are not matching with material study on different AZO and hydrogenated AZO layers. Pseudo-fill factor (pFF), measured with a SunsV_{OC} equipment, are also presented in Figure 10 for front standard AZO and *in situ* hydrogenated AZO. pFF values are similarly superior to 83% for these both conditions, illustrating no difference in shunt effect in the solar cells. Therefore, a difference of contact resistivity between front TCO and polysilicon layers could explain these differences. As it has been observed with double side integration of AZO, front side TCO has a lower impact on fill factor value, allowing to work with less conductive alternative material, such as indium-free materials, without degrading fill factor parameter.

2.4.4 Conversion efficiency analysis

In this study, fill factor seems to be the main parameter influencing conversion efficiency values. A maximum average of 22.3% is obtained with standard AZO integrated only at the cell front side. With this structure, a champion cell at 22.4% efficiency has been obtained, representing a record efficiency for such poly-Si/SiO_x-based double side passivated contacts with high temperature route. Hydrogenated AZO layers by *in situ* and *ex situ* routes respectively exhibit average conversion efficiency of 22.12% and 21.93%. For *ex situ* hydrogenated AZO, there is also an impact of low J_{SC} value, which causes a decrease of the efficiency obtained.

For double side integration of AZO layers, effect of the strong dispersion and of lower conductivity than ITO:H layers on rear side are confirmed regarding conversion efficiency values. Efficiencies are over 21.0% for all cells, with an average of 21.58%. Besides, best cell with double side AZO exhibits 22.0% efficiency, highlighting the high dispersion for this condition. These performance values are however inferior to 0.5% in average when changing the rear TCO, which open the way to zinc-based alternative materials to replace indium in TCO layers.

Regarding the differences between cell parameters and conversion efficiency obtained at the cell level, no benefits are clearly established for hydrogenated AZO compared to standard AZO. Optimization of hydrogenation processes, in particular in the case of *ex situ* processes could enhance cell performances, and are still being developed.

3 Conclusion

In this work, the compatibility of indium-free TCO layers with the efficient contacting of polysilicon on oxide structures has been demonstrated. Hydrogenation treatment on ZnO:Al layers allows to improve material properties (optics, electric). *In situ* and *ex situ* by PIII-H_2 hydrogenation have been studied in this aim. It demonstrates that hydrogen concentration is a key factor to control for improving layer performances. Indeed, with *in situ* way containing low hydrogen concentrations in the deposition chamber, such as 0.5% and 1%, has led to better material properties of the AZO film, whereas a higher concentration of 1.5% does not provide positive effects. In the case of *ex situ* hydrogenation, an acceleration voltage of 2 kV limits the degradation of conductivity while improving effective transmission values. Moreover, annealing of AZO:H at 350°C allows to reach an optimum point for the electrical, optical and passivation properties at the same time. The implementation of these layers (i.e., AZO films with various H contents or implantation energy and reference ITO:H layers) has been realized on the front side of double side poly-Si on oxide passivated contacts solar cells. The best results are obtained with front AZO layers, with a champion cell reaching 22.4% efficiency. Integrating a standard AZO on double side of the structure of interest leads to promising maximum conversion efficiency of 22.0%. These results demonstrate the possibility to reduce indium consumption for the industrial fabrication of high efficiency double-side passivated contacts silicon solar cells.

The team acknowledges the French National Research Agency for funding the Oxygen project (ANR-17-CE05-0035), and the French Environment and Management Agency (ADEME) for co-funding Charles Seron's PhD.

Author contribution statement

Charles SERON, Thibaut DESRUES, Frédéric Jay and Adeline LANTERNE planned and coordinated the different experiments. Charles SERON realized AZO layer depositions and material characterizations. Frédéric JAY realized all ITO layers deposition at CEA-INES. Frank TORREGROSA and Gaël BORVON processed all implantation by PIII-H_2 experiments at IBS. All authors contributed to data interpretation. Thibaut DESRUES, Quentin RAFHAY, Anne KAMINSKI and Sébastien DUBOIS supervised the project and actively contributed to manuscript revisions.

References

1. S.W. Glunz, F. Feldmann, A. Richter et al., The irresistible charm of a simple current flow pattern – 25% with a solar cell featuring a full-area back contact, in *31st Eur Photovolt Sol Energy Conf Exhib* (2015), pp. 259–263

2. Y. Larionova, H. Schulte-Huxel, B. Min et al., Ultra-thin poly-Si layers: passivation quality, utilization of charge carriers generated in the poly-Si and application on screen-printed double-side contacted polycrystalline Si on oxide cells, Sol. RRL **4**, 2000177 (2020)
3. R. Peibst, Y. Larionova, S. Reiter et al., Building blocks for industrial, screen-printed double-side contacted POLO cells with highly transparent ZnO:Al layers, IEEE J. Photovolt. **8**, 719 (2018)
4. S. Reiter, N. Koper, R. Reineke-Koch et al., Parasitic absorption in polycrystalline Si-layers for carrier-selective front junctions, Energy Procedia **92**, 199 (2016)
5. Z.C. Holman, A. Descoeudres, L. Barraud et al., Current losses at the front of silicon heterojunction solar cells, IEEE J. Photovolt. **2**, 7 (2012)
6. J.-P. Niemelä, B. Macco, L. Barraud et al., Rear-emitter silicon heterojunction solar cells with atomic layer deposited ZnO:Al serving as an alternative transparent conducting oxide to In2O3:Sn, Sol. Energy Mater. Sol. Cells **200**, 109953 (2019)
7. M. Lokanc, R. Eggert, M. Redlinger, The availability of indium: the present, medium term, and long term, Renew. Energy (2015), https://doi.org/10.2172/1327212
8. L.-L. Senaud, G. Christmann, A. Descoeudres et al., Aluminium-doped zinc oxide rear reflectors for high-efficiency silicon heterojunction solar cells, IEEE J. Photovolt. **9**, 1217 (2019)
9. B. Hallam, D. Chen, M. Kim et al., The role of hydrogenation and gettering in enhancing the efficiency of next-generation Si solar cells: an industrial perspective, Phys. Stat. Solidi A **214**, 1700305 (2017)
10. M. Lozac'h, S. Nunomura, H. Umishio et al., Roles of hydrogen atoms in p-type poly-Si/SiO_x passivation layer for crystalline silicon solar cell applications, Jpn. J. Appl. Phys. **58**, 050915 (2019)
11. N. Juneja, L. Tutsch, F. Feldmann et al., Effect of hydrogen addition on bulk properties of sputtered indium tin oxide thin films, AIP Conf. Proc. **2147**, 040008 (2019)
12. F. Torregrosa, L. Roux, A. Lanterne et al., PULSION®-Solar, a efficient and cost effective plasma immersion ion implantation solution for phosphorus and boron doping needed for high conversion efficiency silicon solar cells, in *2018 22nd International Conference on Ion Implantation Technology (IIT)* (2018), pp. 180–183
13. T. Desrues, C. Oliveau, C. Seron et al., Doping and Hydrogenation Processes for Passivating Contact Solar Cells Using Plasma Immersion Ion Implantation (PIII) , in *37th Eur. Photovolt. Sol. Energy Conf. Exhib., oct. 2020* (2020), pp. 173–175, https://doi.org/10.4229/EUPVSEC20202020-2AO.6.5
14. F. Meyer, A. Savoy, J.J. Diaz Leon et al., Optimization of front SiN_x/ITO stacks for high-efficiency two-side contacted c-Si solar cells with co-annealed front and rear passivating contacts, Sol. Energy Mater. Sol. Cells **219**, 110815 (2021)
15. E. Bruhat, T. Desrues, D. Blanc-Pélissier et al., Contacting n+ poly-Si junctions with fired AZO layers: a promising approach for high temperature passivated contact solar cells, in *2019 IEEE 46th Photovoltaic Specialists Conference (PVSC)* (2020), https://doi.org/10.1109/PVSC40753.2019.8980652
16. A. Cruz, E.-C. Wang, A.B. Morales-Vilches et al., Effect of front TCO on the performance of rear-junction silicon heterojunction solar cells: Insights from simulations and experiments, Sol. Energy Mater. Sol. Cells **195**, 339 (2019)
17. L. Tutsch, F. Feldmann, J. Polzin et al., Implementing transparent conducting oxides by DC sputtering on ultrathin SiO_x/poly-Si passivating contacts, Sol. Energy Mater. Sol. Cells **200**, 109960 (2019)

Cite this article as: Charles Seron, Thibaut Desrues, Frédéric Jay, Adeline Lanterne, Frank Torregrosa, Gaël Borvon, Quentin Rafhay, Anne Kaminski, Sébastien Dubois, Hydrogenation of sputtered ZnO:Al layers for double side poly-Si/SiO_x solar cells, EPJ Photovoltaics **13**, 8 (2022)